Collective electromagnetic modes for beam-plasma interaction in the whole *k* space

A. Bret,* M.-C. Firpo,† and C. Deutsch‡
Laboratoire de Physique des Gaz et des Plasmas (CNRS-UMR 8578), Université Paris XI, Bâtiment 210, 91405 Orsay cedex, France
(Received 24 November 2003; revised manuscript received 9 March 2004; published 4 October 2004)

We investigate the linear stability of the system formed by an electron beam and its return plasma current within a general framework, namely, for any orientation of the wave vector **k** with respect to the beam and without any *a priori* assumption on the orientation of the electric field with respect to **k**. We apply this formalism to three configurations: cold beam and cold plasma, cold beam and hot plasma, and cold relativistic beam and hot plasma. We proceed to the identification and systematic study of the two branches of the electromagnetic dispersion relation. One pertains to Weibel-like beam modes with transverse electric proper waves. The other one refers to electric proper waves belonging to the plane formed by **k** and the beam, it divides between Weibel-like beam modes and a branch sweeping from longitudinal two-stream modes to purely transverse filamentation modes. For this latter branch, we thoroughly investigate the intermediate regime between two-stream and filamentation instabilities for arbitrary wave vectors. When some plasma temperature is allowed for, the system exhibits a critical angle at which waves are unstable for every k. Besides, in the relativistic regime, the most unstable mode on this branch is reached for an oblique wave vector. This study is especially relevant to the fast ignition scenario as its generality could help clarify some confusing linear issues of present concern. This is a prerequisite towards more sophisticated nonlinear treatments.

DOI: 10.1103/PhysRevE.70.046401 PACS number(s): 52.35.Qz, 52.35.Hr, 52.50.Gj, 52.57.Kk

I. INTRODUCTION

Beam-plasma interactions play a crucial role in various fields of physics and the theoretical study of the linear regime of beam-plasma instabilities forms the basis of most plasma physics textbooks. The long-standing academic development of this field is now being revivified and challenged by some recent technological progress making accessible new physical regimes [1], e.g., in the context of conventional accelerators and free electron lasers, by new observational data and theories in astrophysics [2,3] and especially by the considerable interest in the elaboration of scenarios for the inertial confinement fusion. In the high-intensity laser-driven scheme and specifically in the fast ignition scenario (FIS) first formulated by Tabak *et al.* in Ref. [4], electron beam-plasma interactions play a key role. Actually, the fast ignition eventually involves an intense suprathermal electron beam, produced by the interaction of a femtosecond laser pulse with the dense core plasma, that should propagate across the plasma corona of the fuel target to ensure a local deposit of the energy. In order to validate this scenario, it is important to study the potential beam-plasma instabilities involved. Many theoretical, numerical, and experimental works have been recently devoted to this topic [3,5–14] and, in particular, some authors [7,10] have pointed out the need to analyze the coupling between two-stream and filamentation instabilities.

In this, paper, we shall study the linear stability of the equilibrium state formed by an electron beam and its return plasma current. This system is relevant to the FIS as, when penetrating into the plasma, the electron beam generates the return current carried by the plasma electrons. For this analysis, one operates in the Vlasov-Maxwell framework and derives the dispersion relation in the $(\mathbf{k},\omega)$ space. This requires the choice of a given orientation for **k**. In this regard, the wave-vector orientations normal ("filamentation instability" [3,15–17]) or parallel ("two-stream instability" [15,18,19]) to the beam have been the most investigated. Yet *every orientation* of **k** is obviously present in the $(\mathbf{r},t)$ reality space found back by inverse Fourier transform, summing over all **k**'s and all ω's. The main objective of this paper is, therefore, to investigate analytically a three-dimensional (3D) Vlasov-Maxwell model of these instabilities for any orientation of **k**. In order to clearly display plasma temperature and relativistic effects, we shall study the problem for three different models: (1) cold beam through a cold plasma, (2) cold beam through a hot plasma, and (3) cold relativistic beam through a hot plasma. Ignoring the beam temperature will allow us to neglect potential additional kinetic effects related to wave-particle resonances.

Usual terminology is not always crystal clear, and sometimes somehow confusing, about the respective definition of the Weibel and filamentation instabilities. It is therefore desirable to be definite from the beginning: In this paper, we shall denote by filamentation modes the unstable waves having a wave vector normal to both the beam and the electric field ($\mathbf{k}\perp$ beam, $\mathbf{k}\perp\mathbf{E}$) and by Weibel modes the unstable waves with wave vector parallel to the beam, namely, the preferred direction, and normal to the electric field ($\mathbf{k}\parallel$ beam, $\mathbf{k}\perp\mathbf{E}$). This corresponds to the original Weibel's modes configuration [18]. Purely two-stream modes, as usual, are longitudinal unstable waves with wave vector aligned with the beam ($\mathbf{k}\parallel$ beam, $\mathbf{k}\parallel\mathbf{E}$).

In Sec. II, we expose the derivation of the dielectric tensor for any orientation of the wave vector and any angle between

*Electronic address: antoine.bret@pgp.u-psud.fr
†Electronic address: marie-christine.firpo@pgp.u-psud.fr
‡Electronic address: claude.deutsch@pgp.u-psud.fr

k and **E**, and single out the large wave velocity ω/k regime. We discuss the respective orientations of **k** and **E** and the nature of the waves in Sec. III. We then apply the general electromagnetic formalism to the analysis of a cold beam interacting with a cold plasma in Sec. IV and with a hot plasma in Sec. V. Calculations conducted in this section help elucidate unambiguously relativistic beam effects in Sec. VI. In this respect, an important figure (see Fig. 2) concerning all three models is located towards the beginning of the paper. Conclusions are finally presented in Sec. VII.

II. GENERAL DISPERSION RELATION

A. Basic derivation

We consider a homogeneous, spatially infinite, collisionless, and unmagnetized plasma whose dynamics is ruled by the relativistic Vlasov-Maxwell equations for the distribution function $f(\mathbf{p},\mathbf{r},t)$ and the electromagnetic field

$$\frac{\partial f}{\partial t} + \mathbf{v}\cdot\frac{\partial f}{\partial \mathbf{r}} + q\left(\mathbf{E} + \frac{\mathbf{v}}{c}\times\mathbf{B}\right)\cdot\frac{\partial f}{\partial \mathbf{p}} = 0, \tag{1}$$

$$\text{curl}\ \mathbf{E} = -\frac{1}{c}\frac{\partial \mathbf{B}}{\partial t}, \tag{2}$$

$$\text{curl}\ \mathbf{B} = \frac{1}{c}\frac{\partial \mathbf{E}}{\partial t} + \frac{4\pi}{c}\mathbf{J}, \tag{3}$$

with $\mathbf{v}=\mathbf{p}/(\gamma m_e)$ and $\gamma=\sqrt{1+p^2/(m_e^2c^2)}=1/\sqrt{1-v^2/c^2}$. cgs Gaussian units are used, q is the electron charge, and m_e is its mass. Ions are assumed to form a fixed neutralizing background. Applying Fourier transformation $F(\mathbf{r},t)=\Sigma_{\mathbf{k}}F_{\mathbf{k}}\exp(i\mathbf{k}\cdot\mathbf{r}-i\omega t)$ in the linearized equations and eliminating the perturbed magnetic field gives the basic form of the dispersion relation

$$\frac{\omega^2}{c^2}\varepsilon(\mathbf{k},\omega)\mathbf{E}_{\mathbf{k}} + \mathbf{k}\times(\mathbf{k}\times\mathbf{E}_{\mathbf{k}}) = \mathbf{0}. \tag{4}$$

The expression of the dielectric tensor $\varepsilon(\mathbf{k},\omega)$ is

$$\varepsilon(\mathbf{k},\omega) = \mathbf{I} + \frac{4\pi q^2}{\omega}\int d\mathbf{p}\frac{\mathbf{v}}{\omega-\mathbf{k}\cdot\mathbf{v}}\frac{\partial f_0(\mathbf{p})}{\partial \mathbf{p}}\cdot\left[\left(1-\frac{\mathbf{k}\cdot\mathbf{v}}{\omega}\right)\mathbf{I} + \frac{\mathbf{k}\otimes\mathbf{v}}{\omega}\right], \tag{5}$$

where $\mathbf{k}\otimes\mathbf{v}=(k_iv_j)$ denotes the tensorial product of **k** and **v**. This yields the following expression of the dielectric tensor elements [17,20]:

$$\varepsilon_{\alpha\beta} = \delta_{\alpha\beta} + \frac{\omega_{\text{pe}}^2}{n_e\omega^2}\int\frac{p_\alpha}{\gamma}\frac{\partial f_0}{\partial p_\beta}d^3p + \frac{\omega_{\text{pe}}^2}{n_e\omega^2}\int\frac{p_\alpha p_\beta}{\gamma}\frac{\mathbf{k}\cdot\partial f_0/\partial\mathbf{p}}{m_e\gamma\omega-\mathbf{k}\cdot\mathbf{p}}d^3p, \tag{6}$$

where the integrals must be evaluated using the standard Landau contour for a proper kinetic treatment. It is worth noticing that the second left-hand side term reduces to $-\omega_{\text{pe}}^2/\omega^2\delta_{\alpha\beta}$ in the nonrelativistic limit, where ω_{pe} is the plasma frequency given by $\omega_{\text{pe}}=q\sqrt{4\pi n_e/m_e}$.

B. Preliminary analysis

At this stage, we may emphasize a point concerning the respective orientation of **k** and **E** that has some bearings on the dispersion relation (4). If one makes the electrostatic approximation and neglects the magnetic field so that $\mathbf{k}\times\mathbf{E}\simeq 0$, the dielectric tensor takes the much simpler form

$$\varepsilon(\mathbf{k},\omega) = 1 + \frac{4\pi q^2}{k^2}\int\frac{\mathbf{k}\cdot\partial f_0(\mathbf{p})/\partial\mathbf{p}}{\omega-\mathbf{k}\cdot\mathbf{v}}d^3p. \tag{7}$$

Moreover the basic dispersion relation (4) simplifies dramatically when considering longitudinal or transverse waves. For longitudinal waves (see, e.g., Refs. [20,21]), the dispersion relation reduces to

$$\varepsilon(\mathbf{k},\omega)\mathbf{E}_{\mathbf{k}} = 0. \tag{8}$$

When considering transverse waves [10,17,18] for which $\mathbf{k}\cdot\mathbf{E}_{\mathbf{k}}=0$, one has $\mathbf{k}\times(\mathbf{k}\times\mathbf{E}_{\mathbf{k}})=-k^2\mathbf{E}_{\mathbf{k}}$ and Eq. (4) yields the dispersion relation for purely transverse waves

$$\left[\frac{\omega^2}{c^2}\varepsilon(\mathbf{k},\omega) - k^2\mathbf{I}\right]\mathbf{E}_{\mathbf{k}} = 0. \tag{9}$$

Without any assumption upon the nature of the waves, we set $\mathbf{k}\times(\mathbf{k}\times\mathbf{E}_{\mathbf{k}})=(\mathbf{k}\cdot\mathbf{E}_{\mathbf{k}})\mathbf{k}-k^2\mathbf{E}_{\mathbf{k}}$ in Eq. (4) and get

$$\left[\frac{\omega^2}{c^2}\varepsilon(\mathbf{k},\omega) + \mathbf{k}\otimes\mathbf{k} - k^2\mathbf{I}\right]\mathbf{E}_{\mathbf{k}} = \mathbf{0}. \tag{10}$$

Setting

$$\mathbf{T} = \frac{\omega^2}{c^2}\varepsilon(\mathbf{k},\omega) + \mathbf{k}\otimes\mathbf{k} - k^2\mathbf{I}, \tag{11}$$

nontrivial ($\mathbf{E}_{\mathbf{k}}\neq 0$) solutions are obtained provided that $\det(\mathbf{T})=0$, i.e.,

$$\det\left|\frac{\omega^2}{c^2}\varepsilon_{ij} + k_ik_j - k^2\delta_{ij}\right| = 0. \tag{12}$$

This forms the most general expression of the dispersion relation.

We can now start to detail the geometry of our problem. The momentum distribution anisotropy is set along the z axis (see Fig. 1 for clarity). Without any restriction of generality, cylindrical symmetry allows us to set $\mathbf{k}=(k_x,0,k_z)$. We shall use in the sequel electronic equilibrium distribution functions f_0 of the type

$$f_0(\mathbf{p}) = f_0(p_x^2+p_y^2,p_z) = f_{0x}(p_x^2)f_{0y}(p_y^2)f_{0z}(p_z), \tag{13}$$

with $\int f_0(\mathbf{p})d^3p=n_e$. These distribution functions are isotropic in the (x,y) plane. We can notice that Eq. (13) implies a vanishing average momentum in the (x,y) plane. Due to its generality, this framework addresses filamentation [3,15] as well as double-stream [15] instabilities. Under the above assumptions, Eq. (12) reduces to

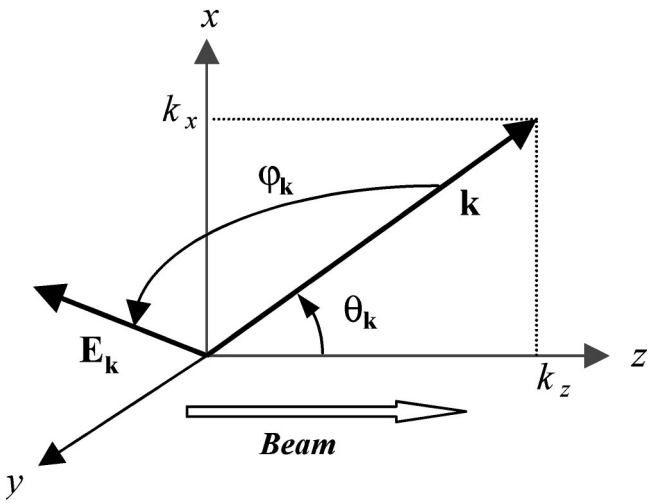

FIG. 1. Geometry of the problem. The angle $\varphi_{\mathbf{k}}$ between the electric field mode $\mathbf{E}_{\mathbf{k}}$ and the wave vector $\mathbf{k}$ may take all values between 0 and $\pi/2$.

$$\begin{vmatrix} \eta^2\varepsilon_{xx}-k_z^2 & 0 & \eta^2\varepsilon_{xz}+k_zk_x \\ 0 & \eta^2\varepsilon_{yy}-k^2 & 0 \\ \eta^2\varepsilon_{xz}+k_xk_z & 0 & \eta^2\varepsilon_{zz}-k_x^2 \end{vmatrix} = 0, \quad (14)$$

where $\eta \equiv \omega/c$. Developing the determinant with respect to the second column yields the following general form of the dispersion relation:

$$(\eta^2\varepsilon_{yy}-k^2)[(\eta^2\varepsilon_{xx}-k_z^2)(\eta^2\varepsilon_{zz}-k_x^2)-(\eta^2\varepsilon_{xz}+k_zk_x)^2]=0, \quad (15)$$

which displays two branches, the $\omega=\omega_1(\mathbf{k})$ branch associated to,

$$\eta^2\varepsilon_{yy}-k^2=0 \quad (16)$$

and the $\omega=\omega_2(\mathbf{k})$ branch solving

$$(\eta^2\varepsilon_{xx}-k_z^2)(\eta^2\varepsilon_{zz}-k_x^2)-(\eta^2\varepsilon_{xz}+k_zk_x)^2=0. \quad (17)$$

This result is valid for any orientation of the wave vector and any orientation of the electromagnetic field with respect to the wave vector. Equation (17) can be factorized by ω^2 without any additional approximation giving

$$\omega^2(\varepsilon_{xz}^2-\varepsilon_{xx}\varepsilon_{zz})+c^2(k_z^2\varepsilon_{zz}+2k_xk_z\varepsilon_{xz}+k_x^2\varepsilon_{xx})=0. \quad (18)$$

C. Limit of large-phase velocities

The evaluation of (15) relies on the evaluation of the matrix elements of the dielectric function $\varepsilon(\mathbf{k},\omega)$. Analytical results are difficult to obtain for any orientation. However, a number of conclusions regarding the large-phase velocity ω/k regime can be reached without making explicit the analytical form of the distribution functions. It is clear from (6) that the only nontrivial occurrence of ω in the dispersion equation is the $1/(\omega-\mathbf{k}\cdot\mathbf{v})$ denominator. The momenta run from $-\infty$ to ∞ in the integrals, but are always limited by physical conditions because any distribution function tends to zero rather quickly beyond a threshold velocity V. This quantity usually denotes the thermal velocity in a Maxwellian distribution or a beam velocity if it goes faster than a thermal plasma electron. More generally, V is the higher velocity encountered in a given situation and remains always finite. In the limit $|kV/\omega| \ll 1$, we can expand the denominator inside any integral of the determinant yielding at leading order

$$\varepsilon_{\alpha\beta}=\left(1-\frac{\omega_{\mathrm{pe}}^2}{\omega^2}\right)\delta_{\alpha\beta} \quad (19)$$

so that the dielectric tensor is diagonal. This is consistent with the fact that spatial dispersion vanishes as the distinctive direction $\mathbf{k}$ tends to 0. In this regime, the first dispersion equation (16) reduces to the branch of the usual light waves in plasma [17],

$$\omega^2=\omega_{\mathrm{pe}}^2+k^2c^2. \quad (20)$$

We now turn to the evaluation of the second equation (17). Replacing the $\varepsilon_{\alpha\beta}$'s by their approximated values (19), we get for any orientation of the wave vector

$$(\omega^2-\omega_{\mathrm{pe}}^2)(\omega^2-\omega_{\mathrm{pe}}^2-k^2c^2)=0. \quad (21)$$

Therefore, within the approximations we are using, there are no instabilities in the $|kV/\omega| \ll 1$ regime for any kind of waves. This is a generalization to any orientation of $\mathbf{k}$ of a result previously displayed in [10,17,20].

III. ORIENTATION OF THE WAVES WITH RESPECT TO k

Our analysis so far does not single out transverse from longitudinal waves, even though we derived the simplifications of the general dispersion relation (12) in both cases [see Eqs. (8) and (9)]. To clarify this point, it is important to realize that the system has its own proper waves and that the orientation of the electric field with respect to the wave vector is not a parameter of the problem, but a consequence of the equations. The dispersion relation ensures that 0 is an eigenvalue of the tensor $\mathbf{T}$ defined in Eq. (11), and the eigenvector associated with this eigenvalue is precisely the electric field. We must therefore calculate the angle $\varphi_{\mathbf{k}}$ between $\mathbf{E}_{\mathbf{k}}$ and $\mathbf{k}$ from the equations by making use of the spectral analysis of $\mathbf{T}$.

For distribution functions fulfilling condition (13), the dielectric tensor takes the form given in Eq. (14), that is,

$$\mathbf{T}=\begin{pmatrix} a & 0 & d \\ 0 & b & 0 \\ d & 0 & c \end{pmatrix}, \quad (22)$$

with $a=\eta^2\varepsilon_{xx}-k_z^2$, $b=\eta^2\varepsilon_{yy}-k^2$, $c=\eta^2\varepsilon_{zz}-k_x^2$, and $d=\eta^2\varepsilon_{xz}+k_zk_x$. Being symmetric, $\mathbf{T}$ is diagonal in an eigenvector orthogonal basis. These eigenvectors may be calculated exactly as

$$\mathbf{e}_1 = \begin{pmatrix} 0 \\ 1 \\ 0 \end{pmatrix} \text{ and } \mathbf{e}_{\mathbf{k}\pm} = \begin{pmatrix} a - c \pm \sqrt{\Delta} \\ 0 \\ 2d \end{pmatrix}, \tag{23}$$

where $\Delta = (a-c)^2 + 4d^2$. They are, respectively, associated with the eigenvalues

$$\lambda_1 = b \text{ and } \lambda_\pm = \tfrac{1}{2}(a + c \pm \sqrt{\Delta}), \tag{24}$$

so that, in the eigenvector orthogonal basis $(\mathbf{e}_1, \mathbf{e}_{\mathbf{k}+}, \mathbf{e}_{\mathbf{k}-})$, tensor $\mathbf{T}$ takes the form

$$\mathbf{T} = \begin{pmatrix} \lambda_1 & 0 & 0 \\ 0 & \lambda_+ & 0 \\ 0 & 0 & \lambda_- \end{pmatrix}. \tag{25}$$

One can readily see that the possibility of proper purely transverse waves with the electric field along $\mathbf{e}_1 = \hat{\mathbf{y}}$, namely along the y axis, remains at any orientation of the wave vector with dispersion equation $\lambda_1 = \eta^2 \varepsilon_{yy} - k^2 = 0$, equivalent to the $\omega_1(\mathbf{k})$ branch defined by Eq. (16).

Concerning the $\omega = \omega_2(\mathbf{k})$ branch defined in Eq. (17), one can check that $\lambda_- \lambda_+ = 0$ yields $\omega = \omega_2(\mathbf{k})$. This shows that Eq. (17) can be further factorized. We shall keep on working with it, however, for simplicity since $ac - d^2 = 0$ is more manageable than $\lambda_+ = 0$ or $\lambda_- = 0$.

Let us assume that the conditions for self-excitation of waves along $\mathbf{e}_{\mathbf{k}+}$ or $\mathbf{e}_{\mathbf{k}-}$ are fulfilled, which means $\lambda_+ = 0$ or $\lambda_- = 0$. The simplified expression for both eigenvectors is then readily derived as

$$\mathbf{e}_{\mathbf{k}+}|_{\lambda_+ = 0} = \mathbf{e}_{\mathbf{k}-}|_{\lambda_- = 0} = \begin{pmatrix} -2c \\ 0 \\ 2d \end{pmatrix} \equiv \mathbf{e}_{\mathbf{k}0}(\omega). \tag{26}$$

The expression above does not mean a degeneracy of the eigenvalues because $\lambda_+(\mathbf{k}, \omega)$ and $\lambda_-(\mathbf{k}, \omega)$ do not necessarily vanish together, for the same $(\mathbf{k}, \omega)$ solutions. This expression shows that the $E_{\mathbf{k}x}$ and $E_{\mathbf{k}z}$ components of the self-excited waves electric field satisfy the relation $E_{\mathbf{k}x}/E_{\mathbf{k}z} = -d/a = -c/d$ (since $ac - d^2 = 0$), that is

$$\frac{E_{\mathbf{k}x}}{E_{\mathbf{k}z}} = -\frac{\omega^2 \varepsilon_{zz} - k^2 c^2 \sin^2 \theta_{\mathbf{k}}}{\omega^2 \varepsilon_{xz} + k^2 c^2 \cos\,\theta_{\mathbf{k}} \sin\,\theta_{\mathbf{k}}}, \tag{27}$$

where we set $k_z = k \cos\,\theta_{\mathbf{k}}$ and $k_x = k \sin\,\theta_{\mathbf{k}}$. If we denote by $E_{\mathbf{k}\perp}$ the component of $\mathbf{E}_{\mathbf{k}}$ normal to the wave vector and by $E_{\mathbf{k}\parallel}$ its parallel component, we shift from $(E_{\mathbf{k}x}/E_{\mathbf{k}z})$ to $(E_{\mathbf{k}\perp}/E_{\mathbf{k}\parallel})$ by means of a rotation of angle $\theta_{\mathbf{k}}$, so that

$$\tan\,\varphi_{\mathbf{k}} = \frac{E_{\mathbf{k}\perp}}{E_{\mathbf{k}\parallel}} = \frac{(E_{\mathbf{k}x}/E_{\mathbf{k}z})\cos\,\theta_{\mathbf{k}} - \sin\,\theta_{\mathbf{k}}}{(E_{\mathbf{k}x}/E_{\mathbf{k}z})\sin\,\theta_{\mathbf{k}} + \cos\,\theta_{\mathbf{k}}}. \tag{28}$$

Finally, we can single out the simplest case where the wave vector is parallel to the beam ($\theta_{\mathbf{k}} = 0$, i.e., $k_x = 0$). Since the x and y axes are then symmetric, we have $\varepsilon_{xx} = \varepsilon_{yy}$ and $\varepsilon_{xz} = \varepsilon_{xz} = 0$ so that $\mathbf{T}$ is diagonal with $a = b$ and $d = 0$. It is readily seen that proper waves belonging to the (x, y) plane are governed by the dispersion equation $\eta^2 \varepsilon_{xx} - k^2 = 0$ while proper waves belonging to the z axis are governed by $\varepsilon_{zz} = 0$. Since $\mathbf{k}$ is along z, the first ones are purely transverse while the second are purely longitudinal [which is consistent with equations structures displayed in Eqs. (8) and (9)]. We shall check in the following that within the cold limit approximation, only longitudinal waves can be destabilized (two-stream instability), but temperature-dependent investigations, such as the one conducted in the original work of Weibel, display unstable transverse modes for such wave vectors.

IV. MODEL 1: COLD NONRELATIVISTIC BEAM WITH COLD PLASMA

To solve and analyze the general dispersion relation for an arbitrary equilibrium distribution function is a rather involved task. In order to get some insight about what is going on for oblique wave vectors, we start investigating the $\mathbf{k}$ orientation dependence through the simple model of a cold beam propagating through a cold plasma with return current

$$f_0(\mathbf{p}) = n_\mathrm{p} \delta(p_x)\,\delta(p_y)\,\delta(p_z + P_\mathrm{p}) + n_\mathrm{b} \delta(p_x)\,\delta(p_y)\,\delta(p_z - P_\mathrm{b}). \tag{29}$$

The nonrelativistic relations $P_{\mathrm{p,b}} = m_e V_{\mathrm{p,b}}$ are fulfilled and $n_\mathrm{p} V_\mathrm{p} = n_\mathrm{b} V_\mathrm{b}$ reflects current neutralization. Total density is $n_\mathrm{e} = n_\mathrm{p} + n_\mathrm{b}$. After some calculations, the first dispersion branch (16) yields Eq. (20) for normal light waves in plasma. As for the second dispersion branch (17), we report in Appendix A its complete form in terms of polar coordinates $(k, \theta_{\mathbf{k}})$ in Eq. (B1), where $\theta_{\mathbf{k}}$ measures the angle between the beam velocity and the wave vector (see Fig. 1), and in terms of Cartesian coordinates (k_z, k_x) in Eq. (B2).

Before turning to an arbitrary orientation, we shall start investigating the well-known two-stream (TS) and filamentation (F) instabilities, for $\theta_{\mathbf{k}} = 0$ and $\theta_{\mathbf{k}} = \pi/2$, respectively. We shall make use in the following of the dimensionless variables

$$\Omega = \frac{\omega}{\omega_\mathrm{p}}, \quad Z = \frac{k V_\mathrm{b}}{\omega_\mathrm{p}}, \quad \alpha = \frac{n_\mathrm{b}}{n_\mathrm{p}}, \quad \beta = \frac{V_\mathrm{b}}{c}, \tag{30}$$

where the plasma frequency ω_p refers to the density n_p.

From Eq. (B1) for $\theta_{\mathbf{k}} = 0$, we get the dispersion relation for wave vectors along the beam

$$\left(\Omega^2 - 1 - \alpha - \frac{Z^2}{\beta^2}\right)\left[1 - \frac{\alpha}{(\Omega - Z)^2} - \frac{1}{(\Omega + \alpha Z)^2}\right] = 0, \tag{31}$$

and the usual two-stream dispersion equation is retrieved through the second factor, while the first one yields transverse stable modes. TS longitudinal modes are unstable for $Z < Z_{c0}$ with

$$Z_{c0} = \frac{(1 + \alpha^{1/3})^{3/2}}{1 + \alpha}, \tag{32}$$

and the growth rate reaches its maximum

$$\delta_{m0} \sim \frac{\sqrt{3}}{2^{4/3}}\alpha^{1/3}, \tag{33}$$

for $Z_m \sim 1$ (see Appendix A).

On the other hand, setting $\theta_{\mathbf{k}} = \pi/2$ in Eqs. (B1) and (B2) yields the dispersion equation

$$(\Omega^2 - 1 - \alpha)\left[\Omega^4 - \Omega^2\left(1 + \alpha + \frac{Z^2}{\beta^2}\right) - Z^2\alpha(1+\alpha)\right] = 0. \tag{34}$$

The first factor yields stable modes, and the second polynomial factor has negative imaginary root for any Z. In the limit $\alpha \ll 1$, the growth rate reads

$$\delta_{\pi/2} \sim \beta Z\sqrt{\frac{\alpha}{Z^2+\beta^2}}, \tag{35}$$

that is, $\delta_{\pi/2} \sim \beta\sqrt{\alpha}$ for $Z \gg \beta$. Filamentation instabilities have already been investigated within more complex models [10,15,16]. We checked that the temperature and collision-dependent dispersion equation of Ref. [15] [Eq. (12)] for example, is exactly retrieved in the cold and collisionless limit.

For arbitrarily oriented wave vectors, Fig. 2(a) displays a numerical evaluation of the growth rate in the **k** plane in terms of (Z_z, Z_x). This figure prompts a comment about the opportunity of having a formalism embracing longitudinal and transverse waves. Indeed, the dispersion equation for any angle, assuming the waves longitudinal from the outset, would be the purely TS expression (31) replacing Z by $Z\cos\theta_{\mathbf{k}}$. This would yield a figure quite similar to Fig. 2(a) except in the filamentation direction where the curve profile would just vanish.

To clarify this point, we plotted on Fig. 3 the direction of the unstable electric field modes $\mathbf{E}_{\mathbf{k}}(\omega)$ for $Z_z < 0.5$. It shows that the field vector is aligned with lines passing through the origin, namely, aligned with the wave vector, except near the normal direction. Instead of a discontinuity, there exists a smooth transition domain between purely transverse modes and longitudinal ones. Looking more carefully on how close one needs to be to the Z_x axis to violate the longitudinal wave approximation, we show in Fig. 4(a) a plot of $\cos\varphi_{\mathbf{k}}^2$ with $\varphi_{\mathbf{k}} = (\widehat{\mathbf{k},\mathbf{E}})$. One clearly sees that it significantly departs from 1 for $Z_z \lesssim 0.5$ and $Z_x \sim 0.5$. This shows that the transition domain, where the electrostatic approximation fails, actually covers about one-third of the relevant Z_z range for unstable modes in this Z_x range. Nevertheless, it still describes well the general growth rate properties.

V. MODEL 2: COLD BEAM PASSING THROUGH A HOT PLASMA

We now allow for some temperature effects in the plasma while still considering a nonrelativistic cold beam. This is most simply modeled by changing the plasma part of the electronic distribution (29) to

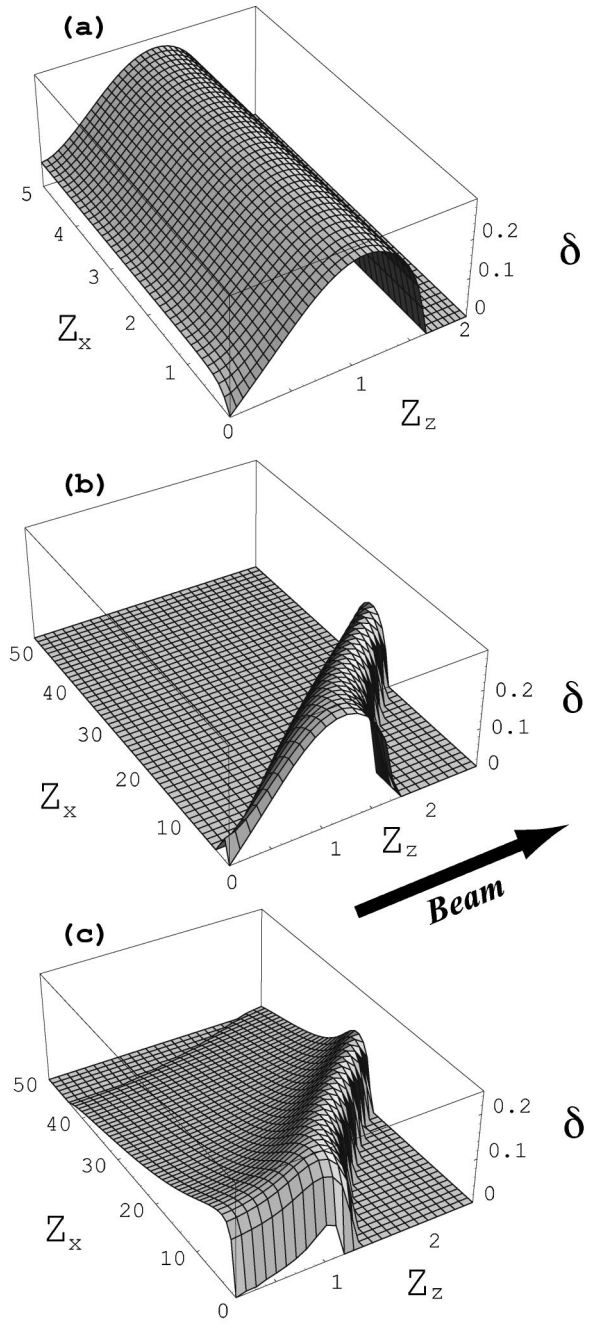

FIG. 2. Numerical evaluation of the two-stream/filamentation growth rate in ω_p units, in terms of $\mathbf{Z} = \mathbf{k}V_b/\omega_p$. (a) Model 1 with $\alpha = 0.1$ and $\beta = 0.2$. (b) Model 2 with $\alpha = 0.1$, $\rho = 0.1$, and $\beta = 0.2$. (c) Model 3 with $\alpha = 0.1$, $\rho = 0.1$, and $\gamma_b = 4$.

$$f_0^p = \frac{n_p}{4P_{th}^2}[\Theta(p_x + P_{th}) - \Theta(p_x - P_{th})] \times [\Theta(p_y + P_{th}) - \Theta(p_y - P_{th})]\delta(p_z + P_p), \tag{36}$$

again with $P_{p,b} = m_e V_{p,b}$ and $n_p V_p = n_b V_b$. $\Theta(x)$ denotes the Heaviside step function. As far as one is not concerned with specific kinetic effects coming through Landau poles, such water-bag distributions provide a classical tool to derive analytical results for temperature effects in relativistic settings

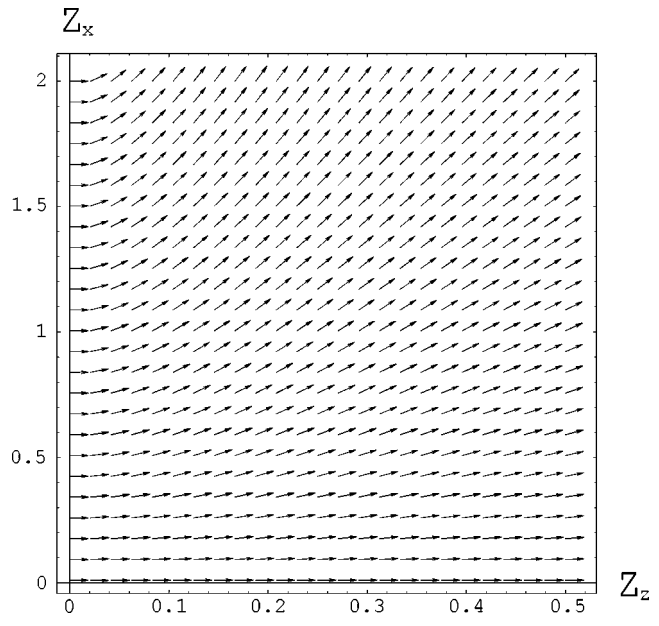

FIG. 3. Direction of the unstable modes electric field $\mathbf{E}(\mathbf{k},\omega)$ for $Z_z<0.5$ and $Z_x<2$ for the cold beam and cold plasma system. Parameters are $\beta=0.2$ and $\alpha=0.1$.

[10,22], and we introduce it here for a similar purpose. We define an additional dimensionless variable measuring plasma temperature

$$\rho = \frac{V_{\mathrm{th}}}{V_{\mathrm{b}}}. \tag{37}$$

The exact dielectric tensor elements calculated for this new distribution function and a relativistic beam are reported in Appendix C. One just needs to set $\gamma_{\mathrm{b}}=1$ in the equations to retrieve the results of this section. This richer system yields a more complex structure of unstable waves, and we now start analyzing separately the two branches defined in Eqs. (16) and (17). The analysis conducted in this section will form a basis for the relativistic beam case.

A. First branch of the dispersion equation: Weibel-like modes

We solve here $\varepsilon_{yy}-k^2c^2/\omega^2=0$. This equation was already displayed in some temperature-dependent investigations [17] while it reduced to some stable modes in the cold previous case. We shall see that it plays a role here due to temperature effects, especially due to the nonvanishing temperature along the y axis [27]. Equation (C1) for the ε_{yy} element yields the dispersion relation $F(\Omega)=0$ with

$$F(\Omega) \equiv P(\Omega) - \frac{1}{3}\frac{\rho^2}{(\Omega/Z+\alpha\ \cos\ \theta_{\mathbf{k}})^2-(\rho\ \sin\ \theta_{\mathbf{k}})^2}, \tag{38}$$

and

$$P(\Omega) = \Omega^2 - 1 - \alpha - \frac{Z^2}{\beta^2}, \tag{39}$$

in terms of the dimensionless variables introduced previously [see Eqs. (30) and (37)].

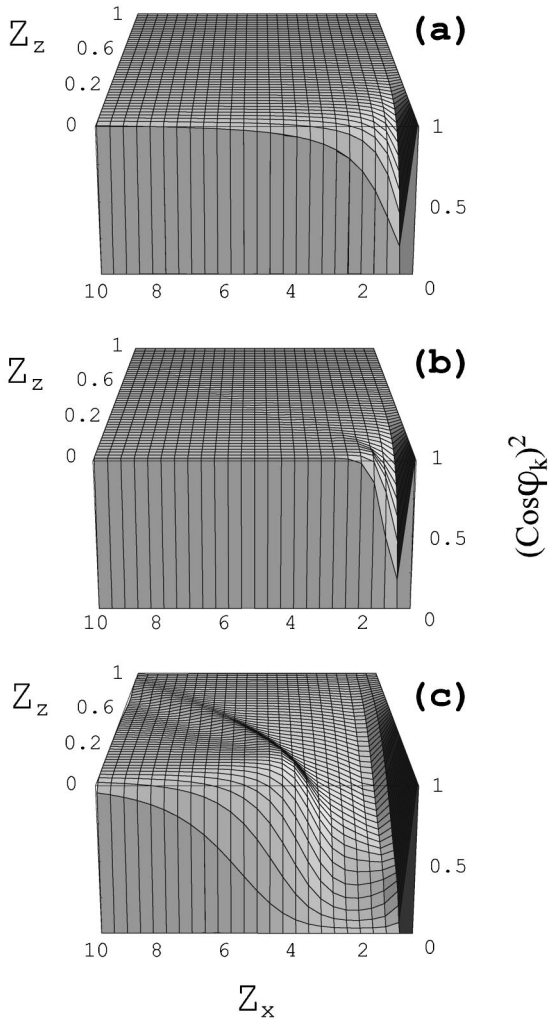

FIG. 4. Plot of $\cos^2\varphi_{\mathbf{k}}$ with $\varphi_{\mathbf{k}}=(\widehat{\mathbf{k},\mathbf{E}})$, in terms of $\mathbf{Z}$ for models 1 (a), 2 (b), and 3 (c). Same parameters as Figs. 2(a)–2(c). The beam is along the Z_z axis.

The temperature dependence in Eq. (38) is clear since $\rho=0$ yields $\omega^2=\omega_{\mathrm{p}}^2+\omega_{\mathrm{b}}^2+k^2c^2$ while a nonzero temperature introduces some rich temperature and angle-dependent features. A quick inspection of Eq. (38) shows that four real roots in $\Omega=\omega/\omega_{\mathrm{p}}$ are required for stability. The function F has two singularities located at $\Omega=-Z\alpha\ \cos\ \theta_{\mathbf{k}}\pm Z\rho\ \sin\ \theta_{\mathbf{k}}$. Instability will appear when the local minimum comprised between those two values becomes positive. This local minimum is roughly reached for $\Omega\sim-Z\alpha\ \cos\ \theta_{\mathbf{k}}$ (the middle of the two singularities) giving the stability condition

$$(Z\alpha\ \cos\ \theta_{\mathbf{k}})^2 + \frac{1}{3\ \sin^2\theta_{\mathbf{k}}} < 1 + \alpha + \frac{Z^2}{\beta^2}. \tag{40}$$

This condition is clearly violated as $\theta_{\mathbf{k}}$ approaches 0. Assuming a weak beam with $\alpha\ll 1$, Eq. (40) means that the waves associated to the first branch are stable for any Z, namely, at any wavelength, provided that $|\sin(\theta_{\mathbf{k}})|>1/\sqrt{3}$. Out of this angle domain, only small-enough wavelength waves, such that $Z>Z_c(\theta_{\mathbf{k}})$, are stable with

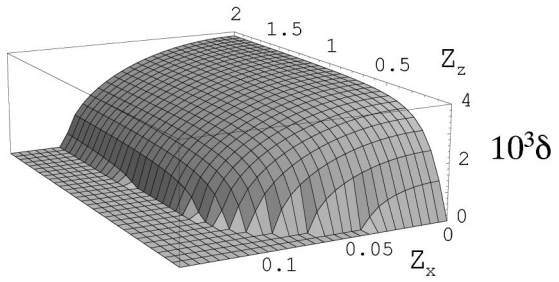

FIG. 5. Numerical evaluation of the first branch growth rate for $\rho=0.03$, $\alpha=0.1$, and $\beta=0.2$. The beam and return current are along the Z_z axis.

$$Z_c(\theta_{\mathbf{k}}) \sim \beta\sqrt{\frac{1}{3\,\sin^2\theta_{\mathbf{k}}}-1}. \tag{41}$$

In the limit $\theta_{\mathbf{k}}\to 0$, that is, for a wave vector almost aligned to the beam, Z_c diverges as $Z_c(\theta_{\mathbf{k}})\sim\beta/(\sqrt{3}|\theta_{\mathbf{k}}|)$. Then all wavelengths are unstable.

The growth rate may be calculated looking for roots under the form $-Z\alpha\cos\theta_{\mathbf{k}}+i\delta$. Assuming δ small and for $\alpha\ll 1$, one gets the following approximate expression at any $\theta_{\mathbf{k}}$:

$$\delta_{1\mathbf{k}} \sim \frac{\rho\beta}{\sqrt{3}}\frac{Z}{\sqrt{Z^2+\beta^2}}\sqrt{1-3\,\sin^2\theta_{\mathbf{k}}}. \tag{42}$$

Figure 5 shows a numerical evaluation of the growth rate in the (Z_x,Z_z) plan. The relative error using Eq. (42) never exceeds 3% so that this formula can be considered as a very good approximation of the growth rate in the whole **k** space. The expression (42) is valid provided that δ is effectively small, namely, for Z small (i.e., large wavelengths) or $\rho\beta$ small. We shall denote this purely transverse mode by W_y.

We observe here an important departure from the cold model where no transverse modes could interact with the electrons for wave vectors along the z axis as no electrons moved perpendicularly to the beam. As temperature introduces such electrons, this set of transverse modes can be destabilized.

In terms of the variables k, ω_{p}, c, and V_{th}, the growth rate (42) for $\theta_{\mathbf{k}}=0$ reads (in ω_{p} units)

$$\delta_1 = \frac{1}{\sqrt{3}}\frac{kV_{\mathrm{th}}}{\sqrt{\omega_{\mathrm{p}}^2+k^2c^2}}, \tag{43}$$

which, dropping the $1/\sqrt{3}$ multiplicative factor, is exactly the original result found by Weibel [18] at low k using a Maxwellian instead of a water-bag electronic equilibrium distribution function for the bulk plasma (without any additional electron beam). Let us remark that the presence of the beam in addition to the bulk plasma prevents the real part of the pulsation from to be null (except for $\theta_{\mathbf{k}}=\pi/2$), which would be one of the features of the original Weibel modes [18].

Let us once more stress here the benefits of the present formalism; being free from the electrostatic approximation, it can describe both longitudinal and transverse waves with wave vectors aligned to the beam direction.

B. Second branch of the dispersion relation for k parallel and k orthogonal to the beam

It is useful to examine the results at both ends of the **k** orientation range before turning to the general case.

1. $\mathbf{k}\|\hat{\boldsymbol{z}}$

When the wave vector is aligned with the beam (along the z axis), so that $k_x=0$ and $k_z=k$, the x and y directions are interchangeable. Therefore, ε_{xz} vanishes and $\varepsilon_{xx}=\varepsilon_{yy}$, as can be checked directly by plugging $\theta_{\mathbf{k}}=0$ in Eq. (C1).

The second factor in Eq. (15) reduces to $\eta^2\varepsilon_{zz}(\eta^2\varepsilon_{xx}-k^2)=0$, that is,

$$\eta^2\varepsilon_{zz}=0, \tag{44}$$

$$\eta^2\varepsilon_{xx}-k^2=0. \tag{45}$$

Using Eq. (C2), the first equation (44) yields the usual two-stream dispersion relation (no temperature corrections here)

$$1-\frac{\alpha}{(\Omega-Z)^2}-\frac{1}{(\Omega+\alpha Z)^2}=0. \tag{46}$$

This is the longitudinal TS mode, unstable for $Z<Z_{c0}$ defined in Eq. (32). The second equation (45) brings

$$\Omega^2\varepsilon_{xx}-\frac{Z^2}{\beta^2}=0, \tag{47}$$

which is identical to Eq. (38) for $\theta_{\mathbf{k}}=0$. This was expected since, for such an orientation of the wave vector, the xx and yy elements of the dielectric tensor are equal. These modes are, therefore, unstable at any Z with growth rates given by the expression δ_1 in Eq. (43). They will be called beam Weibel-like W_{xz} modes.

2. $\mathbf{k}\perp\hat{\boldsymbol{z}}$

Let us now consider wave vectors normal to the beam. After some calculations, the dispersion equation for this branch and this wave vector orientation is found to be $Q_\perp(\Omega)=0$ with

$$Q_\perp(\Omega)\equiv\left(\Omega^2-1-\alpha-\frac{Z^2}{\beta^2}-\frac{\alpha Z^2}{\Omega^2}-\frac{\alpha^2Z^2}{\Omega^2-\rho^2Z^2}\right)\left(\Omega^2-1-\alpha-\frac{\rho^2Z^2}{\Omega^2-\rho^2Z^2}\right)-\left(\frac{\Omega\alpha Z}{\Omega^2-\rho^2Z^2}-\frac{\alpha Z}{\Omega}\right)^2. \tag{48}$$

One can easily check that $Q_\perp$ is an even function of Ω and that the cold limit (35) is retrieved when $\rho=0$. A typical plot of $Q_\perp$ is shown in Fig. 6. Six real roots are needed for stability, and a negative value of $Q_\perp$ at the local minimum located at $\Omega=0$ leads to instability. This value is easily calculated and found positive for $Z>Z_{c\pi/2}$ with

$$Z_{c\pi/2}=\frac{\beta}{\rho}, \tag{49}$$

at leading order in the small parameters β, α, and ρ. A global instability at all wavelengths is retrieved at zero temperature, while plasma temperature stabilizes short-wavelength waves

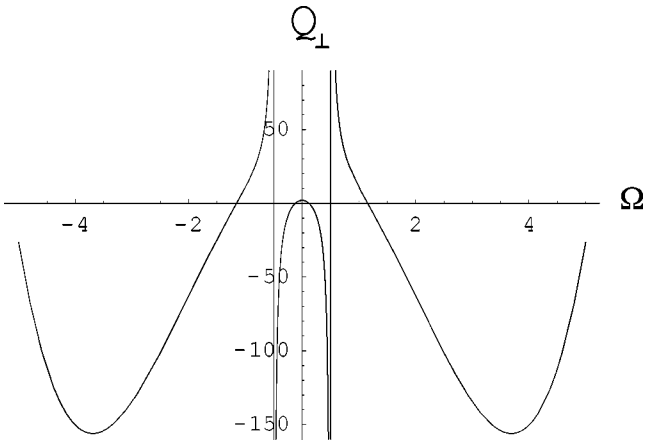

FIG. 6. Typical plot of the dispersion equation (48). The corresponding mode is stable when the local extremum between the singularities is positive.

with $k>(\omega_p/c)(V_b/V_{th})$. This agrees with comparable temperature-dependent investigations [10,22] for wave vectors normal to the beam.

When the stability condition breaks, the corresponding growth rate can be searched by setting $\Omega=i\delta$ in Eq. (48) and by expanding it in powers of δ. This gives

$$\delta_{\pi/2} \sim \beta\sqrt{\alpha}\frac{Z\sqrt{1-Z^2/Z_{c\pi/2}^2}}{\sqrt{(Z^2+\beta^2)(1+\rho^2Z^2)}}, \tag{50}$$

whose maximum is reached for $Z_m \sim \beta/\sqrt{\rho}$ with

$$\delta_{\pi/2}(Z_m) \sim \beta\sqrt{\alpha}. \tag{51}$$

The $\rho=0$ limit of Eq. (50) correctly yields Eq. (35), and one observes that the maximum growth rate (51) equals the growth rate found at zero temperature for $Z \gg \beta$. We shall denote by F modes these almost transverse modes, unstable for $0<Z<Z_{c\pi/2}$.

The effect of temperature has consisted so far in extending the instability domain in the z direction (F is stable for $\rho=0$) while shortening it in the x direction by setting a threshold at $Z\sim\beta/\rho$. We can, therefore, expect a nontrivial border for intermediate orientations bridging between the extremes we have just investigated.

C. Second branch solution for an arbitrary orientation of k: Two-stream/filamentation (TSF) mode

We now consider the $\omega=\omega_2(\mathbf{k})$ branch (17) solving $Q(\Omega,\theta_\mathbf{k})=0$ for any $\theta_\mathbf{k}$, where we introduce

$$Q(\Omega,\theta_\mathbf{k}) \equiv (\hat{\Omega}^2\varepsilon_{xx}-\cos^2\theta_\mathbf{k})(\hat{\Omega}^2\varepsilon_{zz}-\sin^2\theta_\mathbf{k}) - (\hat{\Omega}^2\varepsilon_{xz}+\sin\theta_\mathbf{k}\cos\theta_\mathbf{k})^2. \tag{52}$$

We put here for shortness $\hat{\Omega}\equiv\Omega\beta/Z$ and use the full expression of the dielectric tensor elements (C1). For $\theta_\mathbf{k}=0$, we obtain two unstable modes (in short, W_{xz} and TS) and for $\theta_\mathbf{k}=\pi/2$, only one, mode F (the filamentation mode). We show in this section how the purely longitudinal two-stream arch connects to mode F across the **k** space for the full dispersion branch (52). The Weibel-like beam mode W_{xz} stabilizes when the angle increases and is investigated in the next section.

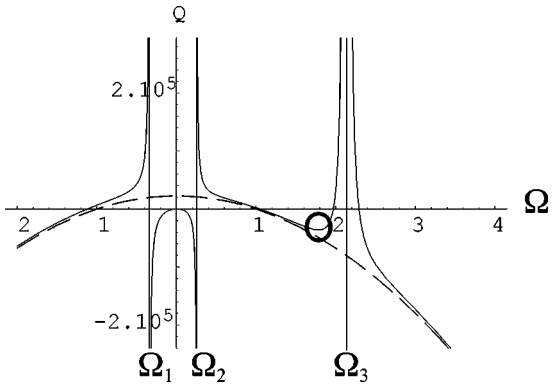

FIG. 7. Plot of $Q(\Omega,\theta_\mathbf{k})$ defined by Eq. (52) as a function of Ω. Parameters are chosen to display clearly the curve topology with $Z=15$, $\beta=0.1$, $\alpha=\rho=0.03$, and $\theta_\mathbf{k}=\pi/2.2$. The circle indicates the place where real roots can appear or disappear. The dashed line is the curve of polynomial $P(\Omega)$ defined by Eq. (53). The Ω_i's are defined by Eq. (54).

Despite its intricate expression, the dispersion relation allows a number of useful analytical conclusions to be drawn. We start noticing that, at large Ω, the asymptotic form of Q must bring the dispersion relation at high frequency (21), so that the polynomial

$$P(\Omega) = (\Omega^2-1-\alpha)(\Omega^2-1-\alpha-Z^2/\beta^2) \tag{53}$$

can be considered as an envelope matching the $Q(\Omega,\theta_\mathbf{k})$ curve except in the vicinity of three singularities located at Ω_1, Ω_2, and Ω_3 with (see Fig. 7)

$$\Omega_1 = -Z\alpha\cos\theta_\mathbf{k} - Z\rho\sin\theta_\mathbf{k},$$

$$\Omega_2 = -Z\alpha\cos\theta_\mathbf{k} + Z\rho\sin\theta_\mathbf{k},$$

$$\Omega_3 = Z\cos\theta_\mathbf{k}. \tag{54}$$

In this section, we shall follow the proper waves having a pulsation real part close to Ω_3, that is, we follow the branch starting at $\theta_\mathbf{k}=0$ with the purely two-stream modes TS. When $\theta_\mathbf{k}$ departs from 0, singularities Ω_1 and Ω_2 separate, as shown in Fig. 7. The "extended" two-stream modes TS are stable as long as the Z-dependent local minimum, marked there by a circle, is negative. Moreover, as $\theta_\mathbf{k}$ keeps increasing, it is clear on Eq. (54) that, due to the plasma transverse temperature, the root Ω_3 will cross the root Ω_2 for some angle below $\pi/2$, and precisely for the critical angle θ_c yielding $\Omega_2=\Omega_3$, that is

$$\theta_c(\alpha,\rho) \equiv \arctan\left(\frac{1+\alpha}{\rho}\right). \tag{55}$$

Let us now depict this more quantitatively. The two zeros of Q on each side of the circle in Fig. 7 are real as long as $P(Z\cos\theta_\mathbf{k})\lesssim 0$ in a first approximation. But unlike the cold plasma model, where this condition is valid all the way

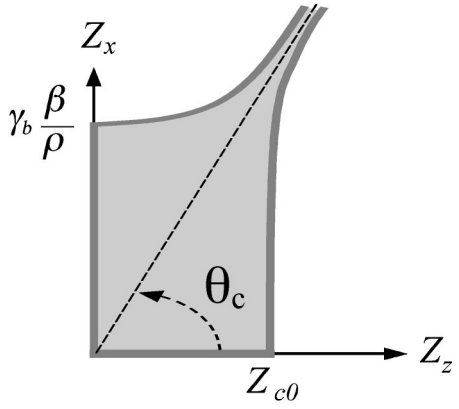

FIG. 8. Stability domain in the $\mathbf{Z}=\mathbf{k}V_b/\omega_p$ plane for the usual two-stream/filamentation mode for model 3. Shaded area corresponds to unstable wave vectors. The angle θ_c is defined through Eq. (55). Setting $\gamma_b=1$ yields model 2 and $\rho=0$ gives model 1 (with $\theta_c \to \pi/2$).

through until $\theta_\mathbf{k}=\pi/2$ [see Fig. 2(a)], the finite plasma temperature case requires us to increase Z higher and higher to recover two real zeros of Q between the Ω_2 and Ω_3 singularities when $\theta_\mathbf{k}$ approaches θ_c. Denoting by $Z_c(\theta_\mathbf{k})$ the instability threshold, this means that $\lim_{\theta_\mathbf{k}\to\theta_c} Z_c(\theta_\mathbf{k})=\infty$. As for an angle larger than θ_c, the proper waves of pulsation close to Ω_3 are stable if the coefficient of $1/(\Omega - Z\cos\theta_\mathbf{k})^2$ in the dispersion equation is positive.

In the limit of small α, β, and ρ, it is possible to derive some analytical results for the stability domain. The leading term of the asymptotic expansion of Z_c for $\theta_\mathbf{k} \lesssim \theta_c$ is found to be [28]

$$Z_c \sim \frac{\sqrt{8\alpha}}{\theta_c - \theta_\mathbf{k}}. \tag{56}$$

Above θ_c, the coefficient of $1/(\Omega - Z\cos\theta_\mathbf{k})^2$ is positive (yielding stability) for [29]

$$Z \geqslant \frac{\beta}{\rho}\sqrt{1+\frac{\pi/2-\theta_\mathbf{k}}{2(\theta_\mathbf{k}-\theta_c)}}, \tag{57}$$

which gives just Eq. (49) for $\theta_\mathbf{k}=\pi/2$. This signifies that one goes continuously from two-stream to filamentation instabilities across the $\mathbf{k}$ plane. Figure 8 displays schematically the stability domain obtained.

The importance of the θ_c direction, at which all spatial scales are unstable, prompts a closer investigation, especially of the growth rate at this angle. Inserting $\Omega = Z\cos\theta_c + i\delta$ with $\delta \ll 1$ into the dispersion function $Q(\delta,\theta_c)$ defined by Eq. (52) gives an expression of the form $\delta^3 Q(\delta,\theta_c) \sim a + b\delta^2$, with $a,b>0$, so that $\delta \sim \sqrt{a/b}$. For small α and ρ, this reads at high Z

$$\delta_{\theta_c} \sim \beta\sqrt{\alpha}. \tag{58}$$

This result bears strong similarities with the growth rate computed for $\theta_\mathbf{k}=\pi/2$ [see Eqs. (50) and (51)]. Indeed, it can also be inferred from a continuity argument: denoting by $\delta^\infty_{\pi/2}$ and $\delta^\infty_{\theta_c}$ the growth rates at high Z in the $\pi/2$ and θ_c directions, both quantities need to merge for $\rho \ll 1$ since $\lim_{\rho\to 0}\theta_c(\rho)=\pi/2$.

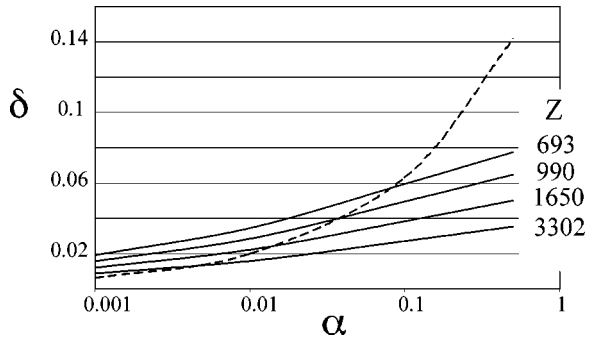

FIG. 9. Maximum growth rate in the θ_c direction in terms of α for Z values up to 3300. The dashed line is the analytical formula (58).

Figure 2(b) shows some numerical evaluation of the growth rate for this hybrid two-stream/filamentation mode. One identifies there both the classical two-stream instability arch along the Z_z axis and the filamentation one along the Z_x axis, but the most remarkable feature of this figure is by far the nondecreasing growth rate in the θ_c direction. Figure 9 displays some numerical computations of the growth rate in the θ_c direction for high Z in terms of α, together with the analytical expression (58). One observes the slow convergence as well as the agreement of this formula at low α.

Finally, we close this investigation by turning to the evaluation of the angle between $\mathbf{k}$ and $\mathbf{E}_\mathbf{k}$ for this mode. A plot of the vector field $\mathbf{E}(\mathbf{k},\omega)$ is presented in Fig. 10. Here again the vector field is almost aligned with the wave vector, except near the normal direction with a transition that sharpens as Z_x increases. We observe a shift in the field direction

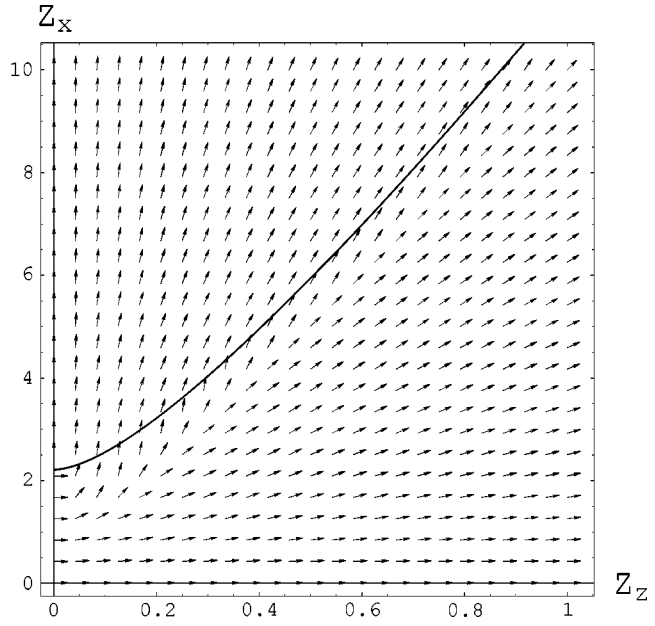

FIG. 10. Direction of the unstable modes electric field $\mathbf{E}(\mathbf{k},\omega)$ for $Z_z<1$ and $Z_x<10$ in the cold beam and hot plasma system. Same parameters as Fig. 2(b). The plain line represents the upper limit of the stability domain.

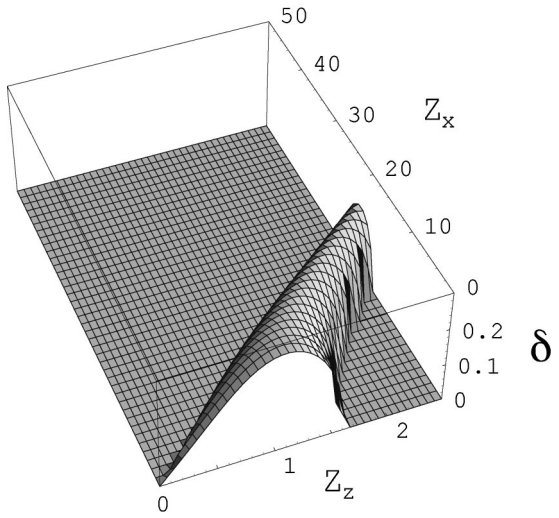

FIG. 11. 3D plot of the growth rate for the two-stream/filamentation mode calculated in the electrostatic approximation using the dielectric tensor [Eq. (7)]. Same parameters as Fig. 2(b).

for wave vectors bordering the upper limit of the stability domain, that is, for almost stable waves. The quantity $\cos \varphi_{\mathbf{k}}^2$ with $\varphi_{\mathbf{k}}=(\widehat{\mathbf{k},\mathbf{E}})$ is displayed on Fig. 4(b) for this model and shows that unstable waves are no longer longitudinal in a region bordering the Z_x axis. Although this region extends up to $Z_z \sim 0.5$ when filamentation is high, the overall growth-rate picture can be recovered from longitudinal approximation as can be seen in Fig. 11, which displays the growth rate calculated in the electrostatic approximation, expressing the dielectric tensor from Eq. (7). Indeed, the critical angle θ_c in the electrostatic approximation is exactly the same. A comparison between Figs. 2(b) and 11 shows that the line $\theta_{\mathbf{k}}=\theta_c$ is the limit beyond which electrostatic approximation fails even qualitatively to describe the growth rate. We shall see this discrepancy between the general electromagnetic approach pursued here and the electrostatic approximation building up when relativistic beam effects are considered.

D. Second branch solution for an arbitrary orientation of k: W_{xz} mode

Having elucidated the two-stream/filamentation mode over the whole **k** domain, we finally consider the Weibel-like beam mode W_{xz} introduced at the beginning of Sec. V B for $\theta_{\mathbf{k}}=0$. In that special case of a wave vector along the beam, the mode was found unstable at any Z (i.e., at any k), with proper pulsations and growth rates identical to those of the first branch mode W_y, and one can expect this similarity to apply to weakly oblique wave vectors for two main reasons. First, because their dispersion equations degenerate exactly for $\theta_{\mathbf{k}}=0$. Secondly, because W_y is always purely transverse and W_{xz} exactly transverse for $\theta_{\mathbf{k}}=0$ and almost transverse after. Actually, the proper electric field modes related to the TSF and W_{xz} branches are normal. Using compact and obvious notations, this means that the TSF eigenvectors $\mathbf{e}_{\mathbf{k}0}(\omega_{\mathrm{TSF}}(\mathbf{k}))$ and the W_{xz} eigenvectors $\mathbf{e}_{\mathbf{k}0}(\omega_{W_{xz}}(\mathbf{k}))$ are orthogonal in the (x,z) plane (see Sec. III).

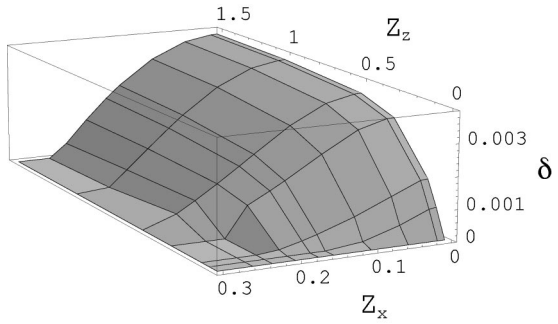

FIG. 12. Numerical evaluation of W_{xz} mode growth rate for $\rho=0.03$, $\alpha=0.1$, and $\beta=0.2$. The beam and return current are along the Z_z axis.

However, the analytical structure of the full dispersion equation is involved, and we restrict ourselves to a numerical computation of the mode growth rate plotted on Fig. 12. This is to be compared to Fig. 5 where the same parameters were used. This calculation exactly confirms the previous analysis. The two surfaces are rigorously equal for $Z_x=0$, and one observes that the stability domain in the Z_x direction is wider for W_{xz} than for W_y.

VI. MODEL 3: COLD RELATIVISTIC BEAM PASSING THROUGH A HOT PLASMA

We finally consider the case of a relativistic beam passing through a hot plasma. The distribution function is exactly the one used in the last section, the only difference being the relativistic factor γ, which may now exceed 1 when calculating tensor elements from Eq. (6). Since our interest lies mainly in the FIS for inertial fusion, we shall keep treating the bulk plasma classically. Its thermal energy is actually expected to be of the order of 10 keV in a fusion plasma and remains much smaller than the 0.5 meV required to tilt relativistic effects. As for the plasma return current velocity V_{p} induced by the relativistic electron beam, its modulus satisfies $V_{\mathrm{p}}/c < n_{\mathrm{b}}/n_{\mathrm{p}}=\alpha$. Yet, it turns out that within the predicted limits of the FIS, α should vary from 10^{-1} (plasma edge) to 10^{-3} (plasma core) [4]. This shows that the return current velocity is nonrelativistic and that it is perfectly relevant to study relativistic effects only for the beam.

Inserting the distribution function [Eq. (29) for the beam part and Eq. (36) for the plasma part] into Eqs. (6) yields the tensor elements reported in Appendix C. The dispersion equation is unchanged and displays the same two branches (16) and (17). We introduce from here the beam relativistic factor

$$\gamma_{\mathrm{b}}=\frac{1}{\sqrt{1-\beta^2}}, \tag{59}$$

with $\beta=V_{\mathrm{b}}/c$.

A. Stability analysis of the first branch: W_y modes for a relativistic beam

Equation (C1) for the ε_{yy} element yields the following expression of the dispersion equation $\omega^2\varepsilon_{yy}-k^2c^2=0$ as

$$P(\Omega) - \frac{1}{3}\frac{\rho^2}{(\Omega/Z + \alpha\cos\theta_{\mathbf{k}})^2 - (\rho\sin\theta_{\mathbf{k}})^2} = 0, \quad (60)$$

with

$$P(\Omega) = \Omega^2 - 1 - \frac{\alpha}{\gamma_b} - \frac{Z^2}{\beta^2}, \quad (61)$$

in terms of the dimensionless variables introduced previously [see Eqs. (30)]. The relativistic correction is very simple and the method used in Sec. V A can be applied straightforwardly. The approximation is even better fulfilled since $\alpha/\gamma_b \ll 1$. Results are, therefore, identical to the ones given by Eqs. (40)–(42) and plotted in Fig. 5.

B. Stability analysis of the second branch: Two-stream/filamentation modes

We shall not investigate further the W_{xz} mode evidenced in Sec. V D. It is very similar to the mode W_y described in Secs. V A and VI A and bears no more relativistic corrections. We therefore turn directly to the two-stream/filamentation mode and shall review the basic results more quickly since their derivation involves the methods used above.

We first emphasize that the expression of the critical angle evidenced in the nonrelativistic case bears no relativistic corrections and remains unchanged here. Actually, its origin lies only in the dispersion relation singularities Ω_i [Eqs. (54)]. Corrections will rather appear in the magnitude of the growth rate.

1. Results for the "privileged" directions $\theta_{\mathbf{k}}=0$, θ_c, and $\pi/2$

For wave vectors normal to the beam ($\theta_{\mathbf{k}}=\pi/2$, filamentation configuration), one finds a dispersion equation yielding unstable modes for $Z < \gamma_b\beta/\rho$ in the limit $\alpha,\rho \ll 1$. This is just the nonrelativistic result times a factor γ_b so that relativistic effects are destabilizing the system at smaller wavelengths. The maximum growth rate in this direction is found for $Z \sim \beta/\sqrt{\rho}$ and reads [22]

$$\delta^R_{m\pi/2} = \beta\sqrt{\frac{\alpha}{\gamma_b}}, \quad (62)$$

where the superscript R stand for relativistic.

For wave vectors along the beam ($\theta_{\mathbf{k}}=0$, two-stream configuration), the dispersion equation yields unstable modes for $Z < 1 + (3/2)\alpha^{1/3}/\gamma_b$ in the limit $\alpha \ll 1$: the relativistic effect is opposite here as it shrinks the instability domain. In the limit $\alpha \ll 1$, the dispersion equation found is formally identical to the nonrelativistic one replacing α by α/γ_b^3. The maximum growth rate is (see [23] and Appendix A)

$$\delta^R_{m0} = \frac{\sqrt{3}}{2^{4/3}}\frac{\alpha^{1/3}}{\gamma_b}. \quad (63)$$

As far as wave vectors in the θ_c direction are concerned, the method used to derive the nonrelativistic asymptotic growth rate in this direction can be applied and brings the asymptotic growth rate

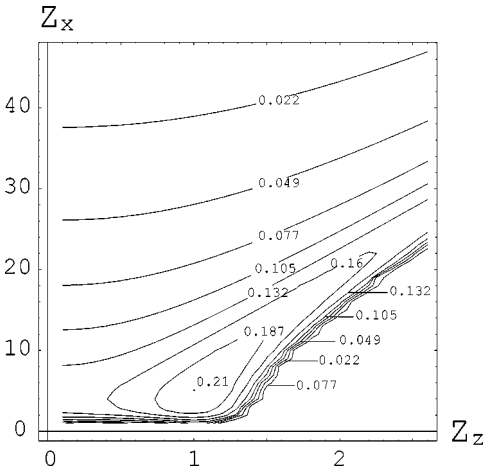

FIG. 13. Contour plot of Fig. 2(c). Maximum growth rate in ω_p units is about 0.21 at $Z_z \sim 1$ and $Z_x \sim 5$. One sees growth rates values of $0.16\omega_p$ up to $Z_x \lesssim 25$ in the θ_c direction.

$$\delta^R_{\theta_c} = \beta\sqrt{\frac{\alpha}{\gamma_b}}. \quad (64)$$

2. Numerical computation of two stream/filamentation growth rates at any **k**

We now turn to the most general case and use the following FIS parameters: a relativistic 2 MeV($\gamma_b=4$) electron beam with density $n_b=10^{20}$ cm^{-3} enters a 10 keV plasma with $n_p=10^{21}$ cm^{-3}. This gives $\alpha=n_b/n_p=0.1$. This values lies in the upper range of α's since electronic plasma density rather ranges from 10^{22} to 10^{26} cm^{-3} within this scenario [4]. These parameters yield a critical angle $\theta_c=\pi/2.12$ that is close to the normal direction.

Figure 2(c) displays a numerical evaluation of the growth rate over the (Z_x,Z_z) plane. One notices the long unstable tail up to $Z_x \sim 40$ in the normal direction as well as the reduced two-stream growth rate in the beam direction. The most striking features are the flat growth rate in the θ_c direction and the maximum reached for $Z_z \sim 1$ and $Z_x \sim 5$. These results are detailed in Fig. 13, which is a contour plot of Fig. 2(c). The angle θ_c between the growth rate's "ridge" and the normal direction is extremely amplified on both figures where the largest wave vector shown is $\mathbf{Z}=(50,2.5)$.

As far as the angle between $\mathbf{k}$ and $\mathbf{E}_{\mathbf{k}}$ is concerned, one can expect here a stronger divergence from the electrostatic approximation. As long as the beam is nonrelativistic, the two-stream growth rate exceeds the filamentation growth rate so that the most unstable modes are longitudinal. On the other hand, the relativistic two-stream and filamentation growth rates scale as $1/\gamma_b$ and $1/\sqrt{\gamma_b}$, respectively. This means that for γ_b high enough, and precisely for

$$\gamma_b > \frac{3}{2^{8/3}\alpha^{1/3}}, \quad (65)$$

filamentation transverse modes are dominant. Numerically, the threshold (65) reads $\gamma_b > 4.7$ for a value as small as $\alpha = 10^{-3}$. Figure 14 shows the growth rate computed within the

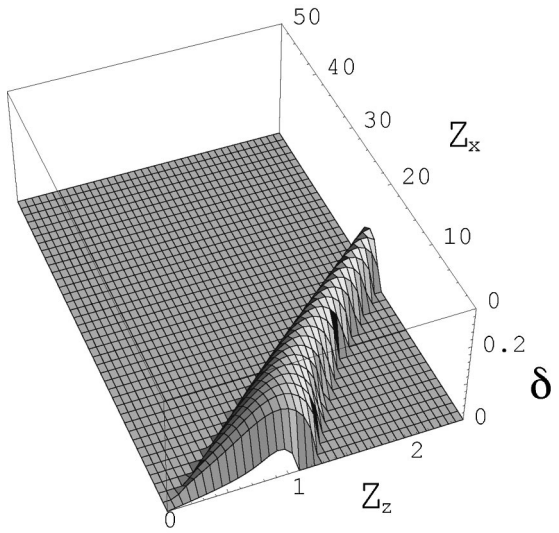

FIG. 14. 3D plot of the growth rate for the two-stream/filamentation mode calculated in the electrostatic approximation using the dielectric tensor [Eq. (7)]. The beam is relativistic with $\gamma_b=4$. Same parameters as Fig. 2(c).

electrostatic approximation for the same parameters as in Fig. 2(c). One can check that the longitudinal model is no longer valid beyond the line $\theta_{\mathbf{k}}=\theta_c$. The angle between $\mathbf{k}$ and $\mathbf{E}_{\mathbf{k}}$ in terms of $\mathbf{k}$ is displayed on Fig. 15 and illustrates this point.

3. Maximum growth rate in the k space

We consider the case $\alpha,\rho \ll 1$ that is relevant to most experimental situations where the beam density is much lower than the target one and the beam velocity is much higher than the target thermal velocity.

The fact that the maximum growth rate is found for an oblique wave vector prompts a closer investigation. Figure 16 displays a comparison of the maximum growth rates in the three privileged directions in terms of γ_b. We used the analytical expressions given in Table I for $\theta_{\mathbf{k}}=0,\pi/2$ and a

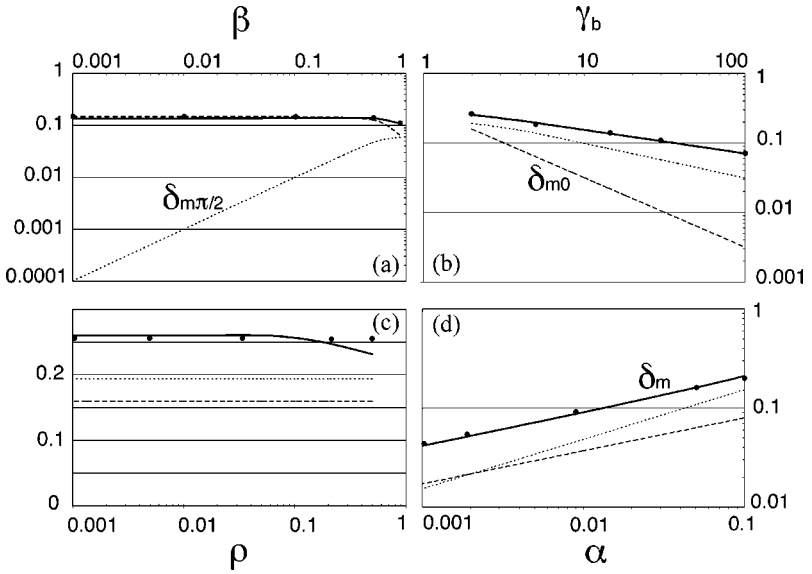

FIG. 16. Comparison between maximum filamentation growth rate ($\delta_{m\pi/2}$, long dashed line), two-stream growth rate (δ_{m0}, short dashed line), and the maximum for all $\mathbf{k}$ (δ_m, plain line) in terms of β, γ_b, ρ, and α. (a) $\alpha=0.1$, $\rho=1/20$. (b) $\alpha=0.1$, $\rho=1/10$. (c) $\alpha=0.1$, $\gamma_b=2$. (d) $\gamma_b=4$, $\rho=0.1$. $\delta_{m\pi/2}$, and δ_{m0} are calculated from Eqs. (62) and (63) while δ_m is numerically evaluated. Black circles are evaluated from Eq. (67).

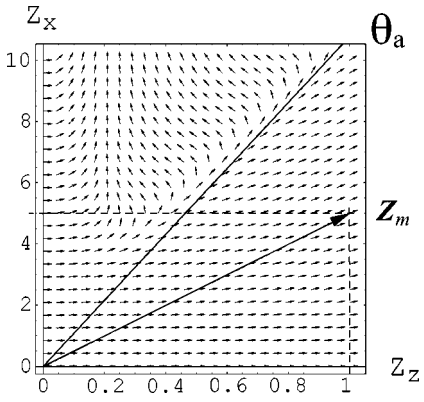

FIG. 15. Orientation of the eigenvector electric field $\mathbf{E}(\mathbf{k},\omega)$ for $Z_z<1$ and $Z_x<10$ in the cold relativistic beam and hot plasma system. Same parameters as Fig. 2(c). We locate θ_c direction as well as the wave vector $\mathbf{Z}_m$ yielding the maximum growth rate.

numerical evaluation of the maximum growth rate.

The $\mathbf{k}$ location of the maximum growth rate can be inferred from a continuity argument when $\rho \ll 1$. It has been proved that, for a cold plasma [24,25], the maximum growth rate dependence on Z_x is weak. The maximum growth rate in the beam direction being always near $Z_z=1$, we can expect this to remain valid in the small temperature limit. A similar argument can apply for the Z_x component of the maximum, showing that it coincides with $Z_x \sim \beta/\sqrt{\rho}$ at which the filamentation growth rate is maximum. Having determined which wave vector $\mathbf{Z}_m$ leads to the maximum growth rate in the relativistic regime, we now make use of Fig. 16 to find an analytical expression for the corresponding growth rate value $\delta_m(\mathbf{Z}_m)$. An analysis of these plots shows that δ_m behaves as $\alpha^{1/3}$ for $\alpha \ll 1$ and as $1/\gamma_b^{1/3}$ in the relativistic regime. Figure 16(c) shows that, in the $\rho \ll 1$ limit, we can guess $\delta_m(Z_m) \propto (\alpha/\gamma_b)^{1/3}$. By continuity arguments with the TS branch, we finally conjecture that the maximal growth rate is reached for

$$\mathbf{Z}_m \sim \left(\frac{\beta}{\sqrt{\rho}},1\right), \tag{66}$$

with

TABLE I. Growth rate properties for each unstable modes within model 3.

Modes	Solution branch[a]	$\varphi_{\mathbf{k}}$[b]	Stability domain	Max. growth rate	Magnitude[c]
W_y (Weibel)	$\lambda_1=0$	$\pi/2$	See Fig. 5	$\rho\beta/\sqrt{3}$	$0.84\beta\rho\gamma_b\alpha^{-1/3}$
W_{xz}	$\lambda_+\lambda_-=0$	$\sim\pi/2$[d]	See Fig. 12	$\rho\beta/\sqrt{3}$[e]	$0.84\beta\rho\gamma_b\alpha^{-1/3}$
TSF	$\lambda_+\lambda_-=0$	$0\rightarrow\pi/2$	See Fig. 8		
$\theta_{\mathbf{k}}=0$		0		$\sqrt{3}/2^{4/3}\alpha^{1/3}/\gamma_b$	1
$\theta_{\mathbf{k}}\sim\arctan(\beta/\sqrt{\rho})$				$\sqrt{3}/2^{4/3}(\alpha/\gamma_b)^{1/3}$	$\gamma_b^{2/3}$
$\theta_{\mathbf{k}}=\theta_c$				$\beta\sqrt{\alpha/\gamma_b}$[f]	$1.45\beta\sqrt{\gamma_b}\alpha^{-1/3}$[f]
$\theta_{\mathbf{k}}=\pi/2$		$\pi/2$		$\beta\sqrt{\alpha/\gamma_b}$	$1.45\beta\sqrt{\gamma_b}\alpha^{-1/3}$

[a]See Eqs. (24) for λ_i definition.
[b]$(\mathbf{k},\hat{\mathbf{E}}_{\mathbf{k}})$ angle.
[c]Normalized to the two-stream (TS) maximal growth rate.
[d]Exactly for $\theta_{\mathbf{k}}=0$.
[e]For $\theta_{\mathbf{k}}=0$.
[f]For $Z\rightarrow\infty$.

$$\delta_m(\mathbf{Z}_m)\sim\frac{\sqrt{3}}{2^{4/3}}\left(\frac{\alpha}{\gamma_b}\right)^{1/3}. \tag{67}$$

Figure 16 shows that this expression fits numerical evaluations very well. As for the $\mathbf{Z}_m$ value, Eq. (66) gives $\mathbf{Z}_m\sim(5.3,1)$, which also fits the value obtained from Figs. 2(c) and 13 very well.

VII. DISCUSSION AND CONCLUSION

We used a general electromagnetic formalism to derive the unstable proper modes, propagating at any wave vector $\mathbf{k}$, associated with the system formed by an electron beam and its return plasma current. Previous analyses restricted us to some special $\mathbf{k}$ direction (parallel or normal to the beam) or to some asymptotic regimes [26] or to make some *a priori* assumptions on the nature of the waves (restricting to the longitudinal or to the transverse case). This work, aided by numerical computations of the dispersion relation, was motivated by the need for a clearer picture of the linear theory for this beam-plasma system relevant to the FIS.

The significance of using an electromagnetic formalism instead of the electrostatic approximation appears from the hot plasma model and becomes evident when taking into account relativistic beam effects. Advantages are numerous. Firstly, it yields a rigorous and coherent description of unstable modes all over the $\mathbf{k}$ space. Secondly, once the distribution function is given, the dielectric tensor spectral analysis allows a systematic search for every possible unstable mode regardless of its $(\widehat{\mathbf{k},\mathbf{E}_{\mathbf{k}}})$ angle. Thirdly, it shows the limitations of the electrostatic approximation by displaying purely transverse modes for a wave vector around the beam axis (W_y and W_{xz}) or normal to it (F). As for the two-stream/filamentation unstable modes, some quantitative discrepancy between the two approaches is confined around the normal direction as long as the filamentation growth rate remains smaller than the two-stream growth rate. This is always the case in the nonrelativistic regime (and small beam density), but the situation changes dramatically with relativistic beam effects when the filamentation growth rate scales as $1/\sqrt{\gamma_b}$ whereas the two-stream growth rate goes like $1/\gamma_b$. A plot of the quantity $\cos^2\varphi_{\mathbf{k}}$ [see Fig. 4(c)] demonstrates that the transition domain between longitudinal two-stream waves and filamentation transverse waves is then no longer confined to the close vicinity of the normal direction. This is also obvious looking at the orientation of the electric field as displayed in Fig. 15.

Our main results are summarized in Table I and eventually display two kinds of instabilities. The first one gathers instabilities for wave vectors along the beam axis and purely (or almost purely) transverse waves while the second one is the two-stream/filamentation mode. The last column displays the relative magnitude of each growth rate normalized to the two-stream maximum growth rate. It appears that the transverse and quasitransverse W_y and W_{xz} modes can be dominant in front of two-stream instability for $\alpha=n_b/n_p$ small enough because their relative magnitude scales as $\beta\rho\gamma_b/\alpha^{1/3}$. As for the two stream/filamentation branch, the two-stream growth rate always exceeds the filamentation growth rate for α and β small. When β tends to one, relativistic effects come into play and filamentation dominates.

On the two stream/filamentation branch, we identified two privileged directions at the angles θ_c and $\arctan(\beta/\sqrt{\rho})$. These modes share properties from filamentation and two-stream instabilities. Like the TS modes, they propagate [30]. The θ_c mode asymptotically shares the filamentation growth rate without being purely transverse. The second mode, which is also the most unstable one, has the two-stream growth rate times $\gamma_b^{2/3}$ without being purely longitudinal. In addition, it "borrows" from filamentation its normal wave vector component and from two-stream its parallel one.

We are currently extending the present methodological framework to include collisions, beam temperature, as well as Maxwellian distribution functions.

ACKNOWLEDGMENT

One of us (A.B.) wishes to thank the Laboratoire de Physique des Gaz et des Plasmas for its hospitality.

APPENDIX A: BASIC RESULTS ON THE TWO-STREAM INSTABILITY

Let us consider the dispersion relation

$$1-\frac{\alpha}{(\Omega-Z)^2}-\frac{1}{(\Omega+\alpha Z)^2}=0, \tag{A1}$$

and operate the change of variable $y\equiv(\Omega-Z)/\alpha^{1/3}$. Then Eq. (A1) turns to the quartic

$$1=\frac{\alpha^{1/3}}{y^2}+[\alpha^{1/3}y+(1+\alpha)Z]^{-2}.$$

With $a\equiv(Z^{-2}-1)\alpha^{-1/3}$, we get

$$\frac{2}{Z^3}y^3-ay^2=1,$$

where we used an expansion in the small parameter α. Putting $y=re^{i\phi}$, we obtain

$$\frac{2}{Z^3}r^3e^{i3\phi}-ar^2e^{i2\phi}=1. \tag{A2}$$

From the imaginary part of Eq. (A2) we get

$$\frac{2}{Z^3}\frac{r\sin(3\phi)}{\sin(2\phi)}=a,$$

which, substituted in the real part of Eq. (A2), gives

$$r^3=-Z^3\cos\phi.$$

We get finally

$$(-\cos\phi)^{1/3}\frac{\sin(3\phi)}{\sin(2\phi)}=\frac{1-Z^2}{2\alpha^{1/3}}\equiv A,$$

$$\frac{\Omega}{Z}=1+\alpha^{1/3}(-\cos\phi)^{1/3}e^{i\phi}.$$

We look for the maximal imaginary value of Ω with respect to A. This occurs for $A=0$, i.e., $Z_m=1$ and gives $\phi=\pi/3$. Then, with $\Omega=\Omega_r+i\delta$, we get the maximal growth rate and associate real part as

$$\Omega_r=1-2^{-4/3}\alpha^{1/3}, \tag{A3}$$

$$\delta_{m0}=\frac{\sqrt{3}}{2^{4/3}}\alpha^{1/3}. \tag{A4}$$

As it is well known, Eq. (A3) shows that the oscillations building up with the largest rate are those whose frequency is close to the plasma frequency (slightly detuned by an amount of the order of the growth rate). Equation (A4) is the result given in Eq. (33). We followed above the line of approach of Bludman *et al.* in Ref. [26].

APPENDIX B: FULL FORM OF EQ. (17)

Inserting the distribution functions introduced by Eq. (29) yields the following expression for Eq. (17):

$$\left(-1+\Omega^2-\alpha-\frac{Z^2\cos^2\theta_{\mathbf{k}}}{\beta^2}\right)\times\left[-1+\Omega^2-\alpha+Z\alpha\frac{-2\Omega\cos\theta_{\mathbf{k}}+Z\cos(2\theta_{\mathbf{k}})}{(\Omega-Z\cos\theta_{\mathbf{k}})^2}+Z\alpha\frac{2\Omega\cos\theta_{\mathbf{k}}+Z\alpha\cos(2\theta_{\mathbf{k}})}{(\Omega+Z\alpha\cos\theta_{\mathbf{k}})^2}-\frac{Z^2\sin^2\theta_{\mathbf{k}}}{\beta^2}\right]-\left[\frac{Z^2\cos\theta_{\mathbf{k}}\sin\theta_{\mathbf{k}}}{\beta^2}+Z\left(\frac{\alpha}{-\Omega+Z\cos\theta_{\mathbf{k}}}+\frac{\alpha}{\Omega+Z\alpha\cos\theta_{\mathbf{k}}}\right)\sin\theta_{\mathbf{k}}\right]^2=0 \tag{B1}$$

It may be useful to write this expression in terms of the **k** Cartesian coordinates (k_z,k_x) instead of polar $(k,\theta_{\mathbf{k}})$. One gets this

$$\left(\Omega^2-1-\alpha-\frac{Z_z^2}{\beta^2}\right)\left[\Omega^2-\alpha\frac{\Omega^2/Z_x^2+1}{(\Omega-Z_z)^2}-\frac{\Omega^2/Z_x^2+\alpha^2}{(\Omega+Z_z\alpha)^2}-\frac{1}{\beta^2}\right]Z_x^2-\left(\frac{\alpha}{-\Omega+Z_z}+\frac{\alpha}{\Omega+Z_z\alpha}+\frac{Z_z}{\beta^2}\right)^2Z_x^2=0, \tag{B2}$$

where as expected

$$Z_z=\frac{k_zV_b}{\omega_p}\quad\text{and}\quad Z_x=\frac{k_xV_b}{\omega_p}.$$

The Z_x^2 factor was left for convenience for it allows a very straightforward retrieval of the $Z_x=0$ or $Z_z=0$ limits. Once simplified, the resulting expression stresses the limited Z_x dependence of the overall dispersion equation.

APPENDIX C: DIELECTRIC TENSOR ELEMENTS $\varepsilon_{\alpha\beta}$

Inserting the equilibrium distribution functions defined in (36) into the expression of the tensor component $\varepsilon_{\alpha\beta}$ given by Eq. (6) yields to the calculation of the tensor elements. They are here expressed without any approximation in terms of the dimensionless variables introduced by Eq. (30). We express for convenience the quantities $\Omega^2\varepsilon_{\alpha\beta}$ as

$$\Omega^2\varepsilon_{xx}=\Omega^2-1-\frac{\alpha}{\gamma_b}-\frac{(\Omega+Z\alpha\cos\theta_{\mathbf{k}})^2\cot^2\theta_{\mathbf{k}}+Z^2\rho^2\sin^2\theta_{\mathbf{k}}}{(\Omega+Z\alpha\cos\theta_{\mathbf{k}})^2-(Z\rho\sin\theta_{\mathbf{k}})^2}-\cot^2\theta_{\mathbf{k}}-\frac{(\Omega+Z\alpha\cos\theta_{\mathbf{k}})\cot^2\theta_{\mathbf{k}}\csc\theta_{\mathbf{k}}}{\rho Z}\Delta, \tag{C1a}$$

$$\Omega^2\varepsilon_{yy}=\Omega^2-1-\frac{\alpha}{\gamma_b}-\frac{1}{3}\frac{Z^2\rho^2}{(\Omega+Z\alpha\cos\theta_{\mathbf{k}})^2-(Z\rho\sin\theta_{\mathbf{k}})^2}, \tag{C1b}$$

$$\Omega^2\varepsilon_{zz}=\Omega^2-1-\frac{\alpha}{\gamma_b^3}+\frac{\alpha Z}{\gamma_b^3}\frac{Z(\cos^2\theta_{\mathbf{k}}-\gamma_b^2\sin^2\theta_{\mathbf{k}})-2\Omega\cos\theta_{\mathbf{k}}}{(\Omega-Z\cos\theta_{\mathbf{k}})^2}-\frac{Z^2\alpha^2}{(\Omega+Z\alpha\cos\theta_{\mathbf{k}})^2-(Z\rho\sin\theta_{\mathbf{k}})^2}-\frac{\alpha\cot\theta_{\mathbf{k}}}{\rho}\Delta, \tag{C1c}$$

$$\Omega^2\varepsilon_{xz} = -\frac{Z\alpha \sin\theta_{\mathbf{k}}}{\gamma_b(\Omega - Z\cos\theta_{\mathbf{k}})} + \cot\theta_{\mathbf{k}} + \frac{Z\alpha(\Omega + Z\alpha\cos\theta_{\mathbf{k}})\csc\theta_{\mathbf{k}}}{(\Omega + Z\alpha\cos\theta_{\mathbf{k}})^2 - (\rho Z\sin\theta_{\mathbf{k}})^2} - \frac{2Z\alpha\cot^2\theta_{\mathbf{k}} + \Omega\cot\theta_{\mathbf{k}}\csc\theta_{\mathbf{k}}}{2\rho Z}\Delta, \quad \text{(C1d)}$$

where

$$\Delta = \ln\left(\left|\frac{\Omega + Z\alpha\cos\theta_{\mathbf{k}} - Z\rho\sin\theta_{\mathbf{k}}}{\Omega + Z\alpha\cos\theta_{\mathbf{k}} + Z\rho\sin\theta_{\mathbf{k}}}\right|\right).$$

The following expansion around $x=0$ can prove useful when one investigates the limits $\theta_{\mathbf{k}}\to 0$ or $\theta_{\mathbf{k}}\to\pi/2$ in Eqs. (C1):

$$\frac{1}{x}\ln\left(\frac{a+kx}{a-kx}\right) = \frac{2k}{a} + \mathcal{O}(x^2). \quad \text{(C2)}$$

[1] S. J. Gilbert, D. H. E. Dubin, R. G. Greaves, and C. M. Surko, Phys. Plasmas **8**, 4982 (2001).
[2] V. Krishan, P. J. Wiita, and S. Ramadurai, Plasma Phys. Controlled Fusion **356**, 373 (2000).
[3] R. A. Fonseca, L. O. Silva, J. W. Tonge, W. B. Mori, and J. M. Dawson, Phys. Plasmas **10**, 1979 (2003).
[4] M. Tabak, J. Hammer, M. E. Glinsky, W. L. Kruer, S. C. Wilks, J. Woodworth, E. M. Campbell, M. D. Perry, and R. J. Mason, Phys. Plasmas **1**, 1626 (1994).
[5] M. Honda, Phys. Rev. E **69**, 016401 (2004).
[6] J. Fuchs, T. E. Cowan, P. Audebert, H. Ruhl, L. Gremillet, A. Kemp, M. Allen, A. Blazevic, J.-C. Gauthier, M. Geissel, M. Hegelich, S. Karsch, P. Parks, M. Roth, Y. Sentoku, R. Stephens, and E. M. Campbell, Phys. Rev. Lett. **91**, 255002 (2003).
[7] M. Tatarakis, F. N. Beg, E. L. Clark, A. E. Dangor, R. D. Edwards, R. G. Evans, T. J. Goldsack, K. W. D. Ledingham, P. A. Norreys, M. A. Sinclair, M.-S. Wei, M. Zepf, and K. Krushelnick, Phys. Rev. Lett. **90**, 175001 (2003).
[8] Y. Sentoku, K. Mima, P. Kaw, and K. Nishikawa, Phys. Rev. Lett. **90**, 155001 (2003).
[9] E. S. Dodd, R. G. Hemker, C.-K. Huang, S. Wang, C. Ren, W. B. Mori, S. Lee, and T. Katsouleas, Phys. Rev. Lett. **88**, 125001 (2002).
[10] L. O. Silva, R. A. Fonseca, J. W. Tonge, W. B. Mori, and J. M. Dawson, Phys. Plasmas **9**, 2458 (2003).
[11] A. Pukhov and J. Meyer-ter-Vehn, Phys. Rev. Lett. **79**, 2686 (1997).
[12] M. Honda, J. Meyer-ter-Vehn, and A. Pukhov, Phys. Rev. Lett. **85**, 2128 (2000).
[13] H. Ruhl, A. Macchi, P. Mulser, F. Cornolti, and S. Hain, Phys. Rev. Lett. **82**, 2095 (1999).
[14] R. A. Fonseca, L. O. Silva, J. Tonge, R. G. Hemker, W. B. Mori, and J. M. Dawson, J. Phys. Chem. Ref. Data Suppl. **30**, 1 (2002).
[15] T. Okada and W. Schmidt, J. Plasma Phys. **37**, 373 (1987).
[16] K. Molvig, Phys. Rev. Lett. **35**, 1504 (1975).
[17] T. Okada, T. Yabe, and K. Niu, J. Phys. Soc. Jpn. **43**, 1042 (1977).
[18] E. S. Weibel, Phys. Rev. Lett. **2**, 83 (1959).
[19] O. Buneman, Phys. Rev. **115**, 503 (1959).
[20] S. Ichimaru, *Basic Principles of Plasma Physics* (Benjamin, Reading, MA, 1973).
[21] L. D. Landau and E. M. Lifshitz, *Course of Theoretical Physics, Physical Kinetics* (Pergamon, New York, 1981), Vol. 10, p. 124.
[22] P. H. Yoon and R. C. Davidson, Phys. Rev. A **35**, 2718 (1987).
[23] R. L. Ferch and R. N. Sudan, Plasma Phys. **17**, 905 (1975).
[24] F. Califano, F. Pegoraro, S. V. Bulanov, and A. Mangeney, Phys. Rev. E **57**, 7048 (1998).
[25] F. Califano, F. Pegoraro, and S. V. Bulanov, Phys. Rev. E **56**, 963 (1997).
[26] S. A. Bludman, K. M. Watson, and M. N. Rosenbluth, Phys. Fluids **3**, 747 (1960).
[27] The evaluation of ε_{yy} from Eq. (6) yields zero in one chooses a distribution function in the v_y direction, such as $\delta(v_y)$, because $\int f(v_y)v_y^2$ is a factor of the whole quantity. The distribution function in this direction plays the very limited role of a multiplicative constant, which cannot be taken to zero, however.
[28] Here are the steps to derive such an expression. (i) Simplifying the dispersion equation around Ω_2 and Ω_3 dropping all terms, which do not depend on Z, as well as the ln's functions which are not the leading terms near singularity Ω_2. When a θ_k depending term behaves smoothly around Ω_2 and Ω_3, the angle is set to $\pi/2$ because $\theta_c \sim \pi/2$. (ii) Evaluating the resulting expression for $\Omega=(\Omega_2+\Omega_3)/2$. (iii) Finding the condition for this minimum to be negative only keeping the leading divergent term yields Eq. (56) with a quite slow convergence.
[29] We start evaluating the highest divergent term of the dispersion equation near Ω_2. Its coefficient is simplified setting $\theta_{\mathbf{k}}=\pi/2$ for nondivergent quantities and developing the others around $\theta_{\mathbf{k}}=\theta_c$.
[30] The growth rate is the imaginary part of a solution of the dispersion equation. The mode does not propagate when the real part $\Omega_r=0$. For this branch, one has $\Omega_r(Z,\theta_{\mathbf{k}})\sim Z\cos\theta_{\mathbf{k}}$.